SolarPACES 2023, 29th International Conference on Concentrating Solar Power, Thermal, and Chemical Energy Systems

Advanced Materials, Manufacturing, and Components

https://doi.org/10.52825/solarpaces.v2i.795

Published: 03 Feb. 2025

Numerical Investigation of Dual Metal Hydride Bed Based Thermochemical Energy Storage System

Sumeet Kumar Dubey[1], K. Ravi Kumar[1,*], Vinay Tiwari[2], and Umish Srivastva[2]

[1] Department of Energy Science and Engineering, Indian Institute of Technology Delhi, India

[2] Alternate Energy, Indian Oil Corporation R&D Centre, Faridabad, Haryana, India

*Correspondence: K. Ravi Kumar, krk@dese.iitd.ac.in

Abstract. Thermochemical energy storage system is known for good thermal stability and high energy storage density. Metal hydride based thermochemical energy storage systems are reported to store thermal energy at higher temperatures. In this analysis, $NaMgH_2F$ and Mg_2NiH_4 are used as high temperature and low-temperature metal hydrides. One kg of $NaMgH_2F$ is used as thermal energy storage media, while Mg_2NiH_4 is used as hydrogen storage media. The analysis includes the study of energy charging and discharging characteristics with heat transfer phenomenon in metal hydride with variation in thermal conductivity of high temperature metal hydride bed. With the increase in thermal conductivity of high temperature metal hydride bed, the heat transfer between heat transfer fluid and metal hydride bed during the energy charging and discharging process has improved. A marginal increase in thermal energy stored and discharged in/from the metal hydride bed system has been observed with an increase in the thermal conductivity of the metal hydride bed. Thermal energy stored in the MH beds for thermal conductivity of 0.5 W/m K, 0.75 W/m K, and 1 W/mK, are 270.88 kJ, 273.39 kJ, and 274.96 kJ, respectively. The energy desorbed from the system for thermal conductivity 0.5 W/mK, 0.75 W/mK, and 1 W/mK are observed as 251.25 kJ, 258.22 kJ, and 260.57 kJ, respectively. The three cases of thermal conductivity have reported an energy storage efficiency of 92.75%, 94.45%, and 94.77%, respectively.

Keywords: Thermal Energy Storage, High Temperature Metal Hydride, Dual Metal Hydride System

1. Introduction

Renewable energy sources are the future alternatives for fulfilling daily energy needs. Solar energy is being utilized to fulfill domestic and industrial electricity demand using solar Photo Voltaic. Thermal energy requirements in domestic, industrial process heating and power generation share a major fraction in thermal energy requirements. Solar energy's intermittent and diurnal variation requires thermal energy storage (TES) to meet the continuous thermal energy requirements of the above-mentioned applications.

TES are classified as sensible, latent, and thermochemical energy storage systems [1]. Sensible heat storage systems store/release thermal energy by increasing/decreasing the temperature of storage media. Latent heat storage systems store/release thermal energy by changing the phase of the storage media. A thermochemical energy storage system store/release thermal energy in the form of a chemical reaction. Thermochemical energy storage systems are known for having the high energy storage density at higher temperatures

and high storage efficiency. Metal hydride based thermochemical energy storage system is one such system that stores thermal energy by carrying an endothermic reaction where metal hydride gets dissociated into metal alloy and hydrogen. The exothermic reaction between the metal alloy and hydrogen will liberate the energy stored in the chemical process, as shown in the chemical reaction below.

$$MH+\Delta H \leftrightarrow Metal\ alloy+Hydrogen \quad (1)$$

Metal alloys have been studied extensively for TES applications and Magnesium (Mg) based alloys are found more suitable for TES applications because of higher energy storage density, thermal stability, enthalpy of reaction, and relatively lower cost. The study performed on waste heat storage using Mg based metal hydrides for the application of steam generation. The study reported a storage capacity of 9.08 kWh with storage efficiency close to 80% at a temperature of 370 ºC [2]. Another 19 gm Mg hydride system was studied and no significant change in storage density was reported for 20 cycles of thermal energy storage at 420 ºC. Due to the small size of the system, the heat losses were significant, but the authors claimed that increasing the size of the system would reduce the heat losses [3]. Two design configuration of Mg_2Ni alloy based TES systems were compared for the storage density and charding/discrging time. The author summarized that the annular reactor configuration improved the desorption rate significantly without much effect on the storage density [4]. Mg alloyed with Nickel (Ni), Cobalt (Co), and Ferrous (Fe) were studied for the storage characteristics. It was reported that cyclic stability, operating temperature range, and reversibility of the alloyed material have improved as compared to Mg hydride, but the thermal stability decreased [5].

Magnesium Nickel (Mg-Ni) alloy was studied for the charging and discharging characteristics by varying the aspect ratio and number of heat transfer tube (HTF) tubes [6]. The authors concluded that the heat transfer in the metal hydride bed is better for the geometry with lesser radial dimension. The dual bed metal hydride systems are also studied, where the high temperature metal hydride (HTMH) bed is used for TES while the low temperature metal hydride (LTMH) bed is used for hydrogen storage. A study used $NaMgH_2F$ and $TiCr_{1.6}Mn_{0.2}$ as HTMH and LTMH, respectively, verifying the system's feasibility with an energy storage density of 226 kWh/m^3 [7]. Another study using Mg_2FeH_6 and Na_3AlH_6 as HTMH and LTMH, verified the system utilization for the temperature range of 450-500 ºC [8]. The authors reported an energy storage density of 132 kWh/m^3. The same metal hydride pair with fins as an extended surface is used to enhance the heat transfer from the system. The authors reported that an energy storage efficiency of 96% and 90 kWh/m^3 energy storage density was achieved [9]. Mg_2Ni alloy and $LaNi_5$ alloy were used as HTMH and LTMH, respectively. The authors reported 89.4% storage efficiency and 156 kWh/m^3 energy storage density [10]. Mg based alloys were reported as suitable materials for TES applications for temperature ranges of 250 to 550 ºC [11, 12].

In this work, $NaMgH_2F$ and Mg_2NiH_4 are used as HTMH and LTMH, respectively. The energy charging and discharging characteristics, along with heat transfer analysis, are performed in this study. The mass of HTMH is considered as 1 kg for the study of charging and discharging characteristics. The quantity of LTMH is calculated based on the quantity of hydrogen produced by HTMH during the energy absorption process. The details of the geometry considered for analysis are explained in the following sections.

2. Numerical Modelling

A numerical model of coupled metal hydride bed for thermal energy storage is developed using COMSOL Multiphysics. The governing equations, geometry details, initial values, boundary conditions and assumptons made in the analysis of the TES system are explained in this section.

2.1 Governing Equations

The numerical model used mass, momentum, and energy conservation equations for calculating the density, velocity, and temperature of the TES system [6, 10, 13]. The mass balance equation for hydride and hydrogen in the porous domain is represented by Equation (2) and Equation (3), respectively. Equations (4) and (5) represent the expression of the mass source term used in mass balance equations for energy absorption and desorption, respectively. The mass balance equation for the hydrogen flowing in the connecting tube and HTF are represented by Equation (6) and (7), respectively.

$$(1-\varepsilon)\frac{\partial \rho_s}{\partial t} = S_m \tag{2}$$

$$\varepsilon\frac{\partial \rho_g}{\partial t} + \nabla.\left(\rho_g u_g\right) = -S_m \tag{3}$$

$$S_m = C_a \times exp\left(\frac{-E_a}{RT}\right) \times \left(\frac{p-p_{eq}}{p_{eq}}\right) \times (\rho_s - \rho_{ini}) \quad \text{for energy absorption} \tag{4}$$

$$S_m = C_d \times exp\left(\frac{-E_d}{RT}\right) \times log\left(\frac{p}{p_{eq}}\right) \times (\rho_{sat} - \rho_s) \quad \text{for energy desorption} \tag{5}$$

$$\frac{\partial \rho_g}{\partial t} + \nabla.\left(\rho_g u_g\right) = 0 \tag{6}$$

$$\frac{\partial \rho_l}{\partial t} + \nabla.\left(\rho_l u_l\right) = 0 \tag{7}$$

The Brinkman equation is used as the momentum balance equation for the hydrogen flow in the porous domain, which is represented by Equation (8). Navier Stokes equation is used as the momentum equation for hydrogen in connecting tube and HTF represented by Equation (9) and (10), respectively.

$$\frac{\rho_g}{\varepsilon}\left(\frac{\partial u_g}{\partial t} + u_g.\frac{\nabla u_g}{\varepsilon}\right) = -\nabla p - \frac{\mu_g}{K}u_g - \frac{S_m}{\varepsilon^2}u_g + \nabla.\left[\frac{\mu_g}{\varepsilon}\left(\nabla u_g + \left(\nabla u_g\right)^T\right) - \frac{2\mu_g}{3\varepsilon}\left(\nabla.u_g\right)\right] \tag{8}$$

$$\left(\frac{\partial u_g}{\partial t} + u_g.\frac{\nabla u_g}{\varepsilon}\right) = -\nabla p + \nabla.\left[\mu_g\left(\nabla u_g + \left(\nabla u_g\right)^T\right) - \frac{2\mu_g}{3}\left(\nabla.u_g\right)\right] \tag{9}$$

$$\left(\frac{\partial u_l}{\partial t} + u_l.\frac{\nabla u_l}{\varepsilon}\right) = -\nabla p + \nabla.\left[\mu_l(\nabla u_l + (\nabla u_l)^T) - \frac{2\mu_l}{3}(\nabla.u_l)\right] \tag{10}$$

The energy balance equations used for the porous domain, hydrogen in the flow tube, and HTF flow is represented by Equation (11), (15), and (16). The system's effective thermal conductivity and heat capacity is calculated based on the volume average of the domain, represented by Equation (12) and (13), respectively. Equation (14) represents the energy source term, i.e., the volumetric energy absorption rate.

$$\left(\rho c_p\right)_{eff}\frac{\partial T}{\partial t} + \rho c_{pg}\left(u_g.\nabla T\right) = \nabla.\left(\lambda_{eff}\nabla T\right) + S_T \tag{11}$$

$$\lambda_{eff} = \varepsilon\lambda_g + (1-\varepsilon)\lambda_s \tag{12}$$

$$\left(\rho c_p\right)_{eff} = \varepsilon\left(\rho c_p\right)_g + (1-\varepsilon)\left(\rho c_p\right)_s \tag{13}$$

$$S_T = S_m(\Delta h) \tag{14}$$

$$\left(\rho_g c_{pg}\right)\left(\frac{\partial T}{\partial t} + u_g.\nabla T\right) = \nabla.\left(\lambda_g \nabla T\right) \tag{15}$$

$$\left(\rho_l c_{pl}\right)\left(\frac{\partial T}{\partial t} + u_l.\nabla T\right) = \nabla.(\lambda_l \nabla T) \quad (16)$$

2.2 Assumptions

The following assumptions have been considered in the numerical analysis of energy absorption and desorption in the dual metal hydride bed system [14].

- Hydrogen gas is assumed as an ideal gas.
- Hydrogen gas and metal hydride bed are in thermal equilibrium.
- Metal hydride material is considered homogenous and isotropic.
- Heat transfer due to radiation is not considered inside the metal hydride bed.
- The thermal properties of metal hydride, hydrogen gas, and heat transfer fluid are considered constant.
- The outer surface of the metal hydride bed is assumed to be perfectly insulated; thus, the heat loss to the surroundings is neglected.

2.3 Geometric Parameters

The coupled geometry considered from the analysis is shown in Figure 1 below.

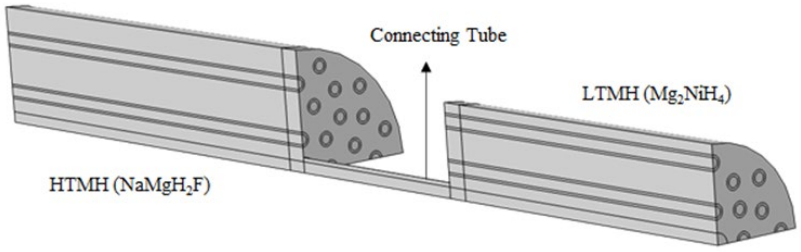

***Figure 1**. A schematic of coupled metal hydride bed system.*

The detailed dimensions of the HTMH, LTMH bed, HTF tubes, and connecting tube are listed in Table 1.

***Table 1.** Geometric parameters of the computational domain [14].*

Parameter	**$NaMgH_2F$ (HTMH)**	**Mg_2NiH_4 (LTMH)**
Diameter of metal hydride bed (mm)	104	79
Height of metal hydride bed (mm)	208	158
Diameter of hydrogen supply tube (mm)	9.5	9.5
Inner diameter of heat transfer fluid tube (mm)	4.4	4.4
Outer diameter of heat transfer fluid tube (mm)	6.4	6.4
Number of heat transfer fluid tubes	44	24

2.4 Initial Values and Boundary Conditions

The initial values of the different domains of the TES system for charging and discharging are listed in Tables 2 and 3, respectively.

Table 2. *Initial values of different domains for the TES charging process.*

Parameter	$NaMgH_2F$ (HTMH)	Mg_2NiH_4 (LTMH)
Initial temperature of MH bed and HTF (K)	873	659.6
Initial pressure of metal hydride bed (bar)	26.09	18.84
Initial temperature of hydrogen in supply tube (K)	298	298
Initial pressure of hydrogen in supply tube (bar)	1	1
Initial pressure of heat transfer fluid (bar)	1	1
Initial density of metal hydride bed (kg/m^3)	1424.75	3200

Table 3. *Initial values of different domains for the TES discharging process.*

Parameter	$NaMgH_2F$ (HTMH)	Mg_2NiH_4 (LTMH)
Initial temperature of MH bed and HTF (K)	823	659.6
Initial pressure of metal hydride bed (bar)	11.61	18.84
Initial temperature of hydrogen in supply tube (K)	298	298
Initial pressure of hydrogen in supply tube (bar)	1	1
Initial pressure of heat transfer fluid (bar)	1	1
Initial density of metal hydride bed (kg/m^3)	1390	3315.2

3. Results and Discussion

The energy absorption and desorption characteristics of dual metal hydride systems using $NaMgH_2F$ and Mg_2NiH_4 as HTMH and LTMH, are studied. The alteration in the composition of metal alloy have resulted in improvement in thermal conductivity of metal alloy. The study of temperature variation in the cross section of the MH bed along the axial length has been performed with different values of thermal conductivity of HTMH.

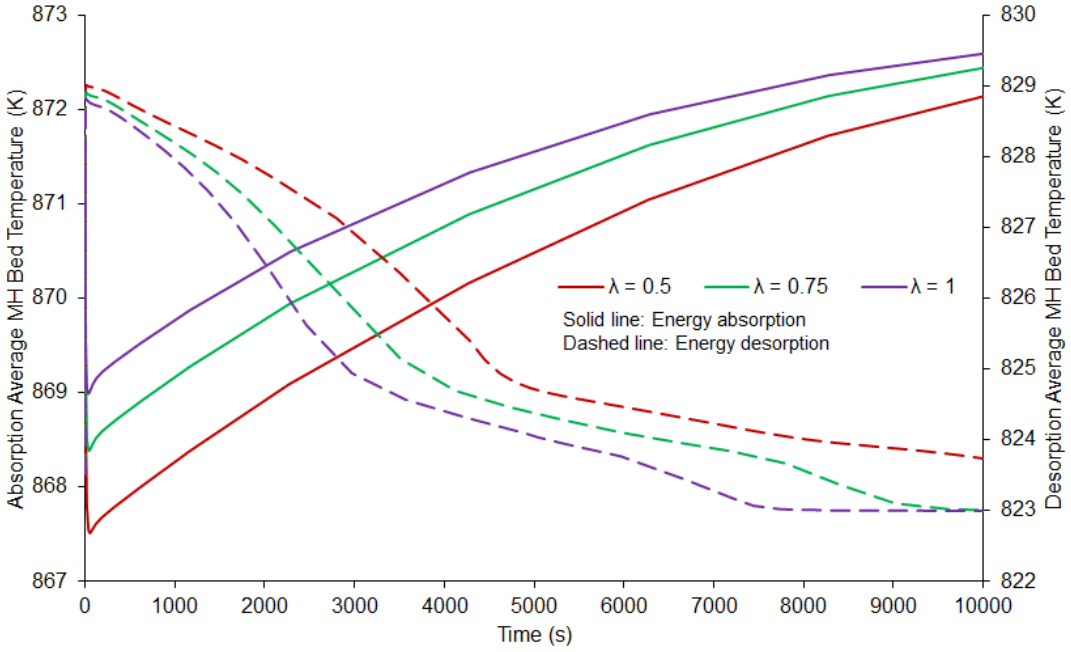

Figure 2*. Variation of HTMH bed average temperature during absorption and desorption.*

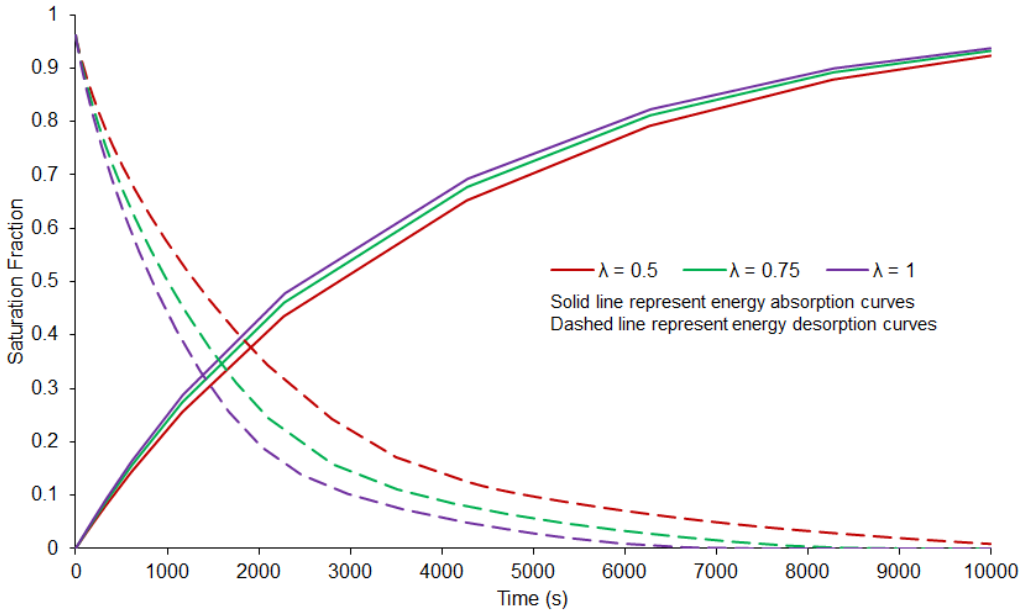

***Figure 3**. Variation of saturation fraction of HTMH bed during absorption and desorption.*

Figure 2 represents the average HTMH bed temperature variation with thermal conductivity during the absorption and desorption processes. The solid line represents the curves for energy absorption while the dashed line represents the curves of energy desorption. Red, green and violet color lines represents the variation for thermal conductivity 0.5 W/m K, 0.75 W/m K, and 1 W/m K, respectively.

With the increase in thermal conductivity of the metal hydride bed, the heat supply rate during energy absorption and heat extraction during energy desorption has increased marginally. During energy absorption, the heat supply to the metal hydride bed has improved with an increase in thermal conductivity and therefore the temperature drop in the metal hydride bed is lesser. The energy absorbed in the MH bed for thermal conductivity 0.5 W/m K, 0.75 W/m K, and 1 W/m K are observed as 270.88 kJ, 273.39 kJ, and 274.96 kJ, respectively. Similarly, during energy desorption, heat extraction improves with the increase in thermal conductivity, and the metal hydride bed with higher thermal conductivity has a lower average bed temperature. while the energy desorbed from the MH bed for thermal conductivity 0.5 W/m K, 0.75 W/m K and 1 W/m K are 251.25 kJ, 258.22 kJ and 260.57 kJ, respectively.

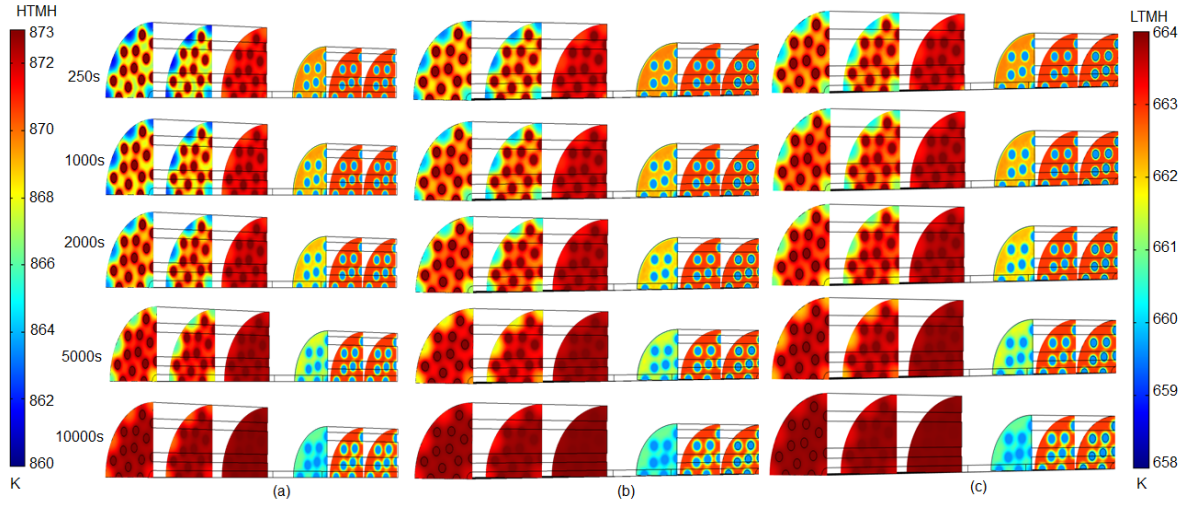

***Figure 4**. Temperature variation along the axial length during energy absorption. (a) 0.5, (b) 0.75, and (c) 1 (W/m K)*

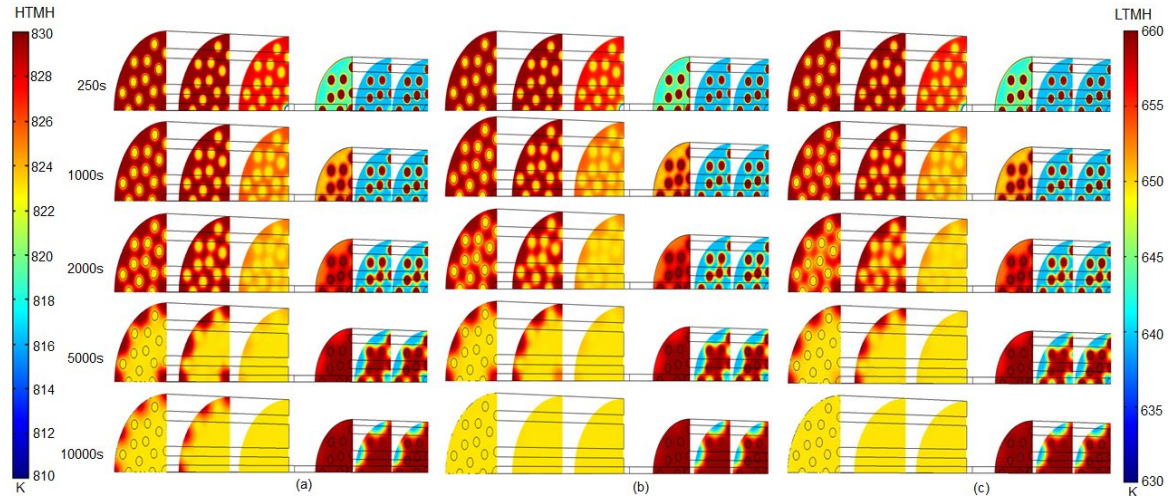

***Figure 5**. Temperature variation along the axial length during energy desorption (a) 0.5, (b) 0.75, and (c) 1 (W/m K).*

Faster absorption and desorption rates have been observed with an increase in the thermal conductivity of the metal hydride bed, as shown in Figure 3.The temperature contours (Figures 4 and 5) also show relatively uniform temperatures in the MH bed cross section for higher thermal conductivity MH bed. The rate of temperature distribution in the cross section of the MH bed has increased due to better heat transfer with the increase in thermal conductivity of MH. The left temperature scale in temperature contour represents the HTMH temperature while right side scale represents the LTMH temperature both in K.The three cases of thermal conductivity have reported an energy storage efficiency of 92.75%, 94.45%, and 94.77%, respectively, as shown in Figure 6.The better heat transfer has resulted in better thermal energy storage efficiency.

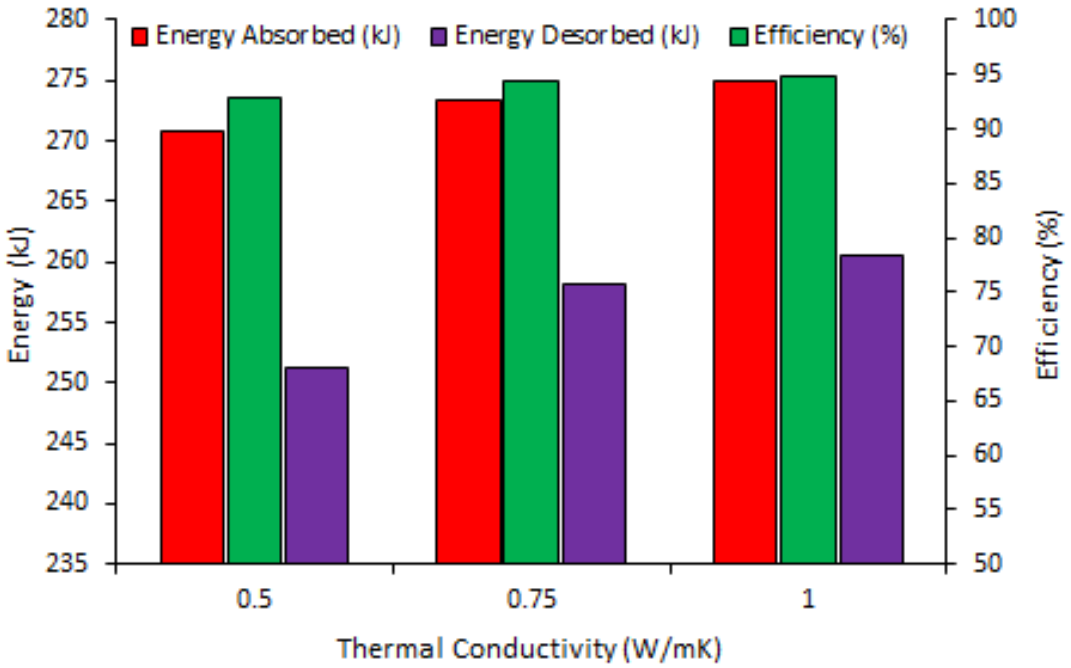

***Figure 6**. Energy absorbed, desorbed, and efficiency for different thermal conductivity.*

4. Conclusions

The heat transfer improvement due to increase in the thermal conductivity of HTMH has shown better energy storage characteristics. The key takeaway of the analysis are as follow:

- The increase in thermal conductivity of the metal hydride bed has improved the heat transfer rate in the bed.
- The energy absorbed in the MH bed for thermal conductivity 0.5 W/m K, 0.75 W/m K, and 1 W/m K are 270.88 kJ, 273.39 kJ, and 274.96 kJ, respectively.
- The energy desorbed in the MH bed for thermal conductivity 0.5 W/m K, 0.75 W/m K, and 1 W/m K are 251.25 kJ, 258.22 kJ, and 260.57 kJ, respectively.
- Thermal energy storage efficiency for thermal conductivity 0.5 W/m K, 0.75 W/m K, and 1 W/m K of 92.75%, 94.45%, and 94.77%, respectively.

Author contributions

Sumeet Kumar Dubey: Conceptualization, Methodology, Investigation, Software, Writing – original draft, Visualization, Writing – review & editing. **K. Ravi Kumar**: Conceptualization, Visualization, Supervision, Writing – review & editing. **Vinay Tiwari:** Supervision, Writing – review & editing. **Umish Srivastva:** Supervision, Writing – review & editing.

Competing interests

The authors declare that they have no competing interests.

Acknowledgment

The authors are thankful to the Science and Engineering Research Board (SERB), Department of Science and Technology (DST), for awarding "Prime Minister Fellowship for Doctoral Research" to Mr. Sumeet Kumar Dubey in collaboration with Indian Oil Corporation Limited, Research and Development Centre and kind support from Confederation of Indian Industry (CII).

References

[1] S. Jain, S. K. Dubey, K. R. Kumar, and D. Rakshit, “Thermal Energy Storage for Solar Energy,” in *Fundamentals and Innovations in Solar Energy*, 2021, pp. 167–215. doi: https://doi.org/10.1007/978-981-33-6456-1_9

[2] B. Bogdanović, A. Ritter, B. Spliethoff, and K. Straßburger, “A process steam generator based on the high temperature magnesium hydride/magnesium heat storage system,” *International Journal of Hydrogen Energy*, vol. 20, no. 10, pp. 811–822, 1995, doi: 10.1016/0360-3199(95)00012-3.

[3] M. Paskevicius, D. A. Sheppard, K. Williamson, and C. E. Buckley, “Metal hydride thermal heat storage prototype for concentrating solar thermal power,” *Energy*, vol. 88, pp. 469–477, 2015. doi : https://doi.org/10.1016/j.energy.2015.05.068

[4] J. Sunku Prasad and P. Muthukumar, “Design of metal hydride reactor for medium temperature thermochemical energy storage applications,” *Thermal Science and Engineering Progress*, vol. 37, no. November 2022, p. 101570, 2023. doi: https://doi.org/10.1016/j.tsep.2022.101570

[5] A. Reiser, B. Bogdanović, and K. Schlichte, “Application of Mg-based metal-hydrides as heat energy storage systems,” *International Journal of Hydrogen Energy*, vol. 25, no. 5, pp. 425–430, 2000, doi: 10.1016/S0360-3199(99)00057-9.

[6] S. K. Dubey and K. R. Kumar, “Charging and discharging analysis of thermal energy using magnesium nickel hydride based thermochemical energy storage system,” *Sustainable Energy Technologies and Assessments*, vol. 52, no. PA, p. 101994, 2022, doi: 10.1016/j.seta.2022.101994.

[7] A. D’Entremont, C. Corgnale, B. Hardy, and R. Zidan, “Simulation of high temperature thermal energy storage system based on coupled metal hydrides for solar driven steam power plants,” *International Journal of Hydrogen Energy*, vol. 43, no. 2, pp. 817–830,

2018, doi: 10.1016/j.ijhydene.2017.11.100.

[8] A. D'Entremont., C. Corgnale, M. Sulic, B. Hardy, R. Zidan, and T. Motyka, "Modeling of a thermal energy storage system based on coupled metal hydrides (magnesium iron – sodium alanate) for concentrating solar power plants," *International Journal of Hydrogen Energy*, vol. 42, no. 35, pp. 22518–22529, 2017. doi: https://doi.org/10.1016/j.ijhydene.2017.04.231

[9] Sofiene Mellouli, F. Askri, A. Edacherian, T. Alqahtani, S. Algarni, J. Abdelmajid, and P. Phelan, "Performance analysis of a thermal energy storage based on paired metal hydrides for concentrating solar power plants," *Applied Thermal Engineering*, vol. 144, pp. 1017–1029, 2018, doi: https://doi.org/10.1016/j.applthermaleng.2018.09.014

[10] K. Malleswararao, A. N, S. Srinivasa Murthy, and P. Dutta, "Performance prediction of a coupled metal hydride based thermal energy storage system," *International Journal of Hydrogen Energy*, vol. 45, no. 32, pp. 16239–16253, 2020, doi: 10.1016/j.ijhydene.2020.03.251.

[11] B. Bogdanović, K. Bohmhammel, B. Christ, A. Reiser, K. Schlichte, R. Vehlen, and U. Wolf, "Thermodynamic investigation of the magnesium-hydrogen system," *Journal of Alloys and Compounds*, vol. 282, no. 1–2, pp. 84–92, 1999, doi: 10.1016/S0925-8388(98)00829-9.

[12] A. Reiser, B. Bogdanovic, and K. Schlichte, "The application of Mg-based metal-hydrides as heat energy storage systems," *International Journal of Hydrogen Energy*, vol. 25, no. 5, pp. 425–430, 2000, doi: https://doi.org/10.1016/S0360-3199(99)00057-9.

[13] S. K. Dubey and K. R. Kumar, "Numerical investigation of energy desorption from magnesium nickel hydride based thermal energy storage system," *Journal of Energy Systems*, vol. 6, no. 2, pp. 165–175, 2022, doi: 10.30521/jes.952627.

[14] S. K. Dubey, K. R. Kumar, V. Tiwari, and U. Srivastava, "Numerical Investigation of Energy Absorption in Dual Metal Hydride Bed based Thermo-Chemical Energy Storage System," 2022. doi: 10.18086/eurosun.2022.13.07.